HHS Public Access

Author manuscript

Int J Radiat Oncol Biol Phys. Author manuscript; available in PMC 2019 November 15.

Published in final edited form as:

Int J Radiat Oncol Biol Phys. 2018 November 15; 102(4): 969–977. doi:10.1016/j.ijrobp.2017.12.269.

Adaptive boost target definition in high-risk head and neck cancer based on multi-imaging risk biomarkers

Feifei Teng[1,5], **Madhava Aryal**[1], **Jae Lee**[1], **Choonik Lee**[1], **Xioajin Shen**[1], **Peter Hawkins**[1], **Michelle Mierzwa**[1,4], **Avraham Eisbruch**[1], and **Yue Cao'**[1,2,3]

[1]Department of Radiation Oncology, University of Michigan, Ann Arbor, MI

[2]Department of Radiology, University of Michigan, Ann Arbor, MI

[3]Department of Biomedical Engineering, University of Michigan, Ann Arbor, MI

[4]Department of Radiation Oncology, Ann Arbor VA Hospital

Abstract

Purpose—^{18}F-deoxyglucose (FDG) PET, dynamic contrast enhanced (DCE) and diffusion weighted (DW) MRI each identify unique risk factors for treatment outcomes in head-and-neck cancer (HNC). Clinical trials in HNC largely rely on a single imaging modality to define targets for boosting. This study aimed to investigate spatial correspondence of FDG uptake, perfusion and apparent diffusion coefficient (ADC) in HNC and their response to chemoradiation therapy (CRT), and to determine implication of this overlap or lack thereof for adaptive boosting.

Materials and methods—Forty patients with HNC enrolled in a clinical trial had FDG-PET/CT pre-CRT, and DCE and DW MRI scans pre and during CRT. Gross tumor volume (GTV) of primary tumor was contoured on post-Gd T1-weighted images. Tumor subvolumes with high FDG uptake, low blood volume (BV), and low ADC were created by using previously established thresholds. Spatial correspondences between subvolumes were analyzed using Dice coefficient and between each pair of image parameters at voxel-level were analyzed by Spearman's rank correlation coefficient.

Results—Prior to CRT, median subvolumes of high FDG, low BV and low ADC relative to primary GTV were 20%, 21% and 45%, respectively. Spearman's correlation coefficients between BV and ADC varied from −0.47 to 0.22, between BV and FDG from −0.08 to 0.59, and between ADC and FDG from −0.68 to 0.25. Dice coefficients between subvolumes of FDG and BV, FDG and ADC, and BV and ADC were 10%, 46%, and 15%, respectively. The union of the three parameters was 64% of GTV. The union of the subvolumes of BV and ADC was 56% of GTV pre-CRT, but reduced significantly by 57% after 10 fractions of RT.

[5]Current address: Department of Radiation Oncology, ShanDong Cancer Hospital, Jinan, China

Conclusion—High FDG uptake, low BV and low ADC as imaging risk biomarkers of HNC identify largely distinct tumor characteristics. A single imaging modality may not define the boosting target adequately.

Introduction

Loco-regional failure remains a significant problem in advanced head and neck squamous cell cancer (HNSCC) despite aggressive therapy including concomitant chemoradiation therapy and accelerated radiotherapy.(1-3) Boosting the tumor subvolumes at high risk for treatment failure with high radiation doses has been demonstrated to be feasible and has the potential to improve loco-regional control (LRC).(4-9)

Several physiological and metabolic imaging modalities, most in isolation, have been investigated for prediction of treatment failure in HNSCC.(3, 10-13) Fludeoxyglucose (FDG) positron emission tomography (PET), a marker for glucose metabolism, has shown high FDG uptake associated with poorer prognosis,(7, 11, 12, 14-16) and has been used for boosting target definition in clinical trials.(17) Also, hypoxic PET, and perfusion CT/MRI and diffusion MRI have shown to be biomarkers for outcomes in HNSCC.(3, 18-20) High hypoxic and poorly perfused tumors all have been associated with worse outcomes.(3, 18) Persisting poorly perfused tumors during the early course of RT is associated with high risk for local and regional failure.(18) Diffusion imaging, a measure of water mobility in tissue and sensitive to cellularity, has shown that an increase in apparent diffusion coefficient (ADC) of the HNSCC during RT is associated with positive therapy response.(19-21) Currently, several dose escalation clinical trials are underway.(22) However, most of these clinical trials use a single imaging modality to guide radiation boost volumes, and single imaging modalities are limited to image only one aspect of tumor biology, The spatial relationship between imaging risk-factor parameters in HNSCC are largely unknown.

This study aimed to investigate whether high FDG uptake, low blood volume, and low diffusion coefficient in advanced head and neck tumors have any spatial correspondence and their early responses to RT to determine the implication of this overlap or lack thereof for adaptive boosting strategy.

Materials and Methods

Patients

Forty-four patients with advanced HNSCC were enrolled in an IRB-approved randomized phase II clinical trial between March 2014 and October 2016.(Table 1) This clinical trial aims to improve LRC of poor prognosis advanced HNSCC patients by escalating radiation doses to radioresistant subvolumes of the tumor. The patients underwent pretreatment FDG-PET/CT scans as a part of the standard care. Dynamic contrast enhanced (DCE) T1-weighted and diffusion-weighted (DW) MRI were acquired at pretreatment and after 10 fractions of 2 Gy as a part of the research protocol.

MRI and PET Acquisition

All MRI scans were acquired on a 3T scanner (Skyra, Siemens Healthineers), including anatomic series, post-contrast T1-weighted images, DCE T1-weighted images and DW images. The patients were scanned in the treatment position using individual patient immobilization face mask and bite bar. Post-contrast T1-weighted images were acquired in the axial plane by a 2D fast spin echo sequence with fat saturation, TE/TR=8.4/658 ms, in-plane resolution of 0.875×0.875 mm, slice thickness/gap of 3 mm/10%, and parallel imaging factor of 2. Sixty DCE T1-weighted image volumes were acquired using a 3D gradient echo pulse sequence (TE/TR =0.97/2.73ms, flip angle 10°, voxel size ~1.5×1.5×2.5, Field of view 30×30×18 cm in a sagittal orientation) during an injection of gadolinium-diethylenetriaminepentaacetic acid (Gd-DTPA) of 0.1 mL/kg with a rate of 2 mL/s, followed by 15 mL of saline flush. DW images were acquired by a 2D spin-echo single shot echo-planar pulse sequence (ssEPI) with TE/TR = 58/ 9420ms, spatial resolution ~1.2 × 1.2 × 4.8 mm, b values of 50, 400 and 800 s/mm^2 and parallel imaging factor of 2 in all patients. In the last 16 patients, a readout segmentation of long variable echo-trains (RESOLVE) pulse sequence that reduced geometric distortion (23) was used to acquired additional DW images with b-values of 50 and 800 s/mm^2. Pre-treatment clinical FDG-PET/CT scans were performed by following the standard clinical protocol.(24)

Image Analysis and Registration

The blood volumes (BV) maps were quantified from DCE-MRI by using the modified Tofts model implemented in an in-house XXX Analysis Tool, XXX.(18, 25) The ADC maps were calculated by in-house software from DW images with b-values of 50 and 800 to mitigate the perfusion effect. FDG-PET/CT was co-registered to post-Gd T1-weighted images for each patient using rigid body transformation. Since all MR images were acquired using immobilization masks and bite bars, BV and ADC maps were reformatted by using image coordinates to match voxel-by-voxel to post-Gd T1-weighted images. Target displacement errors between image series were assessed and described below.

Tumor Volumes and Subvolumes

Gross tumor volumes (GTVs) of primary diseases were contoured based on post-Gd T1-weighted images by radiation oncologists. A metabolic subvolume of the primary tumor was defined as FDG SUV greater than 50% of the maximum value, $MTV_{50\%}$. To analyze the influence of threshold, $MTV_{30\%}$ was also created based up 30% of the maximum SUV. A subvolume of the GTV with low BV (LBV) were created using a threshold of BV<7.636 ml/100g reported previously based upon a histogram analysis.(18) In the patients who had large cystic regions, cystic regions were excluded from LBV. The low ADC volume (LADCV) of the GTV was defined as ADC $\leq 1200\times10^{-6}$ mm^2/s but $>0.1\times10^{-6}$ mm^2/s based on the analysis of ADC histogram distributions within the tumors, which is also coincidence with the mean ADC reported by others.(26)

Data and Statistic Analysis

The voxel-by-voxel correlations between FDG uptake, BV and ADC values in each tumor were analyzed by Spearman's rank correlation coefficient (r). The Dice coefficients between

the subvolumes were calculated to evaluate the spatial overlap between a pair of the subvolumes, which describe the percentage overlap between the two compared volumes. Response of the image-phenotype subvolumes to therapy was analyzed by paired t test.

Quantitative Geometric Distortion Assessment

We assessed target displacement errors between ADC maps and post-Gd T1 weighted images acquired by a spin echo sequence. Anatomic landmarks were placed adjacent to or within primary GTVs, and distributed to cover the anterior, posterior, left, right, superior and inferior aspects of the GTV. The numbers of the landmarks varied from 6 to 13 with a median of 9 among all patients.

Results

Gross Tumor Volume and Image-Phenotype Subvolumes of Primary tumor

For the 44 patients enrolled in the trial, all patients had high quality DCE MRI for BV quantification but 4 patients did not have FDG PET images in our system for analysis and 7 patients did not have high quality ADC maps (with median values of target displacement errors greater than 6 mm) due to the susceptibility-effect. Therefore, 40 patients were used for the FDG related analysis but the 33 patients for the ADC related analysis. The clinical information of the 40 patients is summarized in Table 1.

The GTVs and image-phenotype subvolumes (absolute and percentage volume relative to GTV) of the 40 patients pre-CRT and after 2 weeks of CRT are shown in Table 2. The median volumes of GTV, $MTV_{50\%}$, LBV, and LADCV pre-CRT were 66.6, 15.5, 12.1 and 24.3 cc, respectively. Also, 90% of the patients had more than 94% of $MTV_{50\%}$ within the GTV, and 95% of the patients had more than 81% of $MTV_{50\%}$ within the GTV, indicating that only a relatively small portion of tumor volumes with high uptake of FDG in very few patients was not within the post-Gd T1WI-based GTVs, suggesting the MRI-based GTV includes the FDG abnormality. LBV and LADCV were 100% within GTV. There were no statistically significant differences in GTV, MTV, LBV, and LADCV of primary tumors between p16− and p16+.

Spatial Overlap between Image-phenotype Subvolumes of Primary Tumor

Next, we evaluated spatial overlapping between each pair of image-phenotype subvolumes. We found that the median Dice Coefficients were 10.3% (0.0-34.3%) between $MTV_{50\%}$ and LBV, 46.1% (range: 7.2%-73.5%) between $MTV_{50\%}$ and LADCV, and 15.4% (range: 0.0%-68.8%) between LBV and LADCV, suggesting approximately 50% of patients who had 46% or greater spatial overlap between $MTV_{50\%}$ and LADCV but largely distinct image-phenotype subvolumes among other pairs. Representative images are shown in Figure 1.

To further understand spatial relationships between each pair of image parameters, we investigated voxel-level correlations between each pair within individual GTVs of primary tumor without using any threshold values. We found that the Spearman's correlation coefficients (r) between BV and ADC varied from −0.47 to 0.22 with a median of 0.−0.08,

between BV and FDG varied from −0.08 to 0.59 with a median of 0.19, between ADC and FDG varied from −0.68 to 0.25 with a median of −0.37, confirming the low spatial correspondence between the image risk-factor parameters, see scatter plots and water fall plots in Figures 2 and 3, respectively.

To investigate whether tumor growth between PET and MRI scans affect the results, we excluded the patients for whom time intervals between the two scans were greater than three weeks from the analysis, resulting 24 patients who had a median of 4.5 days (range: 0 and 19 days) difference between the two scans. The results were found similarly to the whole patient group (Supplementary table 1), suggesting the time interval between the two scans is unlikely the major factor causing lack of spatial correspondence between the two imaging parameters.

Union of Image-phenotype Subvolumes of Primary Tumor

Next, we investigated the union of each pair and the union of all three of image-phenotype subvlumes as well as their fractional volumes within the GTV. We found that the median unions of $MTV_{50\%}$ and LBV, of $MTV_{50\%}$ and LADCV, of LBV and LADCV, of the three parameters were 24.3, 27.4, 32.1, and 41.3 cc, respectively. The medians and ranges of percentage subvolumes relative to GTV are given in Table 2.

Changes in GTV and Image-Phenotype Subvolumes after 2 weeks of CRT

Finally, we investigated how 2 weeks of CRT changed the GTV and subvolumes of BV and ADC. The GTV, LBV and LADCV of primary tumor were reduced significantly (respective p values of 0.01, 0.01 and 0.0002) by 19.6%, 32.1% and 66.0% (median), respectively, after 2 weeks of CRT compared to pre-RT. The reduction rates in LBV and LADCV were significantly greater than in GTV ($p=0.05$ and $p<0.0001$, respectively), suggesting physiological response occurred earlier than volumetric response as reported before.(13) However, the reduction rate in LADCV was significantly greater than in LBV ($p=0.02$, paired t-test). The changes in the union and overlap of the LBV and LADCV were also significant ($p=0.0002$ and $p=0.04$, respectively), the extents of which are similar to the MTV decrease (~40%) observed over a similar time interval by others.(17) All details are listed in Table 2. Using an average reduction of 50% in all three image-phenotype subvolumes, we had an estimated union of the three of 20.7 cc after 2 weeks of CRT, which was 41.3% of the GTV of primary tumor. Again, we did not observe any significant difference of the changes between p16+ and p16−.

Geometric Distortion in ADC Maps

We quantitatively assessed target displacement errors of ADC maps. Among patients, median displacements of landmarks varied from 5.4 mm to 0.94 mm, and the maximum displacements from 8.6 to 1.8 mm. A histogram of displacements of all landmark points is shown in Figure 4. For the patients included in this analysis, there were no significant differences of target displacement errors between the pulse sequences used ($p>0.5$). Furthermore, we evaluated whether spatial correspondences between image pairs were correlated to the median target displacement errors, and did not find any significance (p values from 0.2 to 0.6) (see supplementary Figure 1).

Discussion

In this study, we investigated whether FDG-PET, DCE-MRI and DW-MRI identified the same or different image-phenotype risk subvolumes in HNSCC since each of the three imaging modalities in isolation has identified unique risk subvolumes for loco-regional failure or outcomes, which formed the basis for the single-modality based clinical trials. We found that the spatial correspondences among FDG SUV, fractional blood volume, and ADC were low in the whole group, and but varied greatly from patient to patient, suggesting largely spatial distinct tumor subvolumes defined by the three imaging modality. Our data suggest that boosting a target based upon a single image-risk factor may not be sufficient. However, boosting the union of the three pre-RT volumes could increase toxicity due to the volume size of the union. While investigating the changes in the GTV and subvolumes after 2 weeks of CRT, we found that the low BV and ADC subvolumes decreased approximately 50-60%, and were significantly greater than the GTVs, which is similar to the reduction rate of the FDG metabolic tumor subvolume observed during the similar time interval.(17) One proposed strategy is to adaptively boost the union of the three at week-2 during CRT, representing the persisting high-risk for failure and reduced by ~50% compared to pre-RT. Further test of the hypothesis will be carried out by the analysis of patterns of failure.

Several previous studies have identified that high FDG uptake, high glycolysis, low perfusion, and high hypoxia in HNC pre-treatment are risk factors for local and regional control, progression free survival or overall survival. (18, 19) (21, 27-41) However, whether these imaging risk factors are independent and have any spatial correlation is largely unanswered. Our study finds the low spatial correlation between FDG uptake and fractional blood volume, which supports the notion of the two imaging risk factors most independent and largely spatial distinct. The next question is how the two imaging risk factors respond to chemoradiation therapy. In a phase I clinical trial,(17) patients received FDG-PET scans at pretreatment and after 8 fractions of RT. Compared to pre-RT, the $MTV_{50\%}$ was significantly reduced by 41% after 8 fractions of treatment, which is approximately ~20% greater than the gross tumor volume reduction in the similar time interval reported by others.(42, 43) The reduction in LBV after 10 fraction of 2 Gy treatment estimated in our clinical trial showed a similar extent to one in the $MTV_{50\%}$. All these suggest metabolic and physiological changes occur earlier than the volumetric change of tumor.

Whether low or high ADC is an imaging risk prognostic factor for HNSCC seems to be controversial.(44-48) However, reporting on the association of an increase in ADC during RT with positive therapy response or better outcome is relatively consistent. Despite that, we observed a modest negative correlation between FDG SUV and ADC (that means low ADC is largely corresponding to high FDG SUV) in approximately 50% of the patients, supporting the notion that high tumor cell density could be associated with high glucose metabolism. However, lack of the correspondence between the two in the other 50% of the patients suggests inter-patient heterogeneity. What we observed the overall correlation between FDG SUV and ADC is similar to but slightly greater than one reported previously. (26) There are other factors affecting FDG uptake and diffusion. FDG uptake could be elevated by inflammation. Micro-necrosis in tumor can alter FDG SUV and ADC value.

ADC is not only influenced by cell density or cellularity. Further investigations are needed to understand FDG uptake and ADC in HNSCC.

Our observation that FDG SUV, fractional blood volume, and apparent diffusion coefficient have low spatial correspondence is consistent with tumor heterogeneity in advanced, poor prognostic (smoker or p16−) head-and-neck cancers. However, the question becomes how we should define the target for dose boosting or painting. Currently, in the most of clinical trials, the target for boosting or adaptive boosting is based upon a single imaging modality. Our analysis indicates that these trials are largely boosting different targets. Also, the non-randomized, single-center trials are unlikely to be able to answer the question – which image modality should be used for boosting. Comparison of patterns of failure with the imaging risk factor maps could shed light on this question.

Our study suggests several strategies for defining the target for dose boosting or painting. One possibility is to boost the overlapped subvolume identified by the three imaging risk factors such as high FDG uptake, poor perfusion and low ADC. Due to lack of spatial correspondence, this subvolume would be very small. Another possibility is to boost the union of the subvolumes identified by the three imaging risk factors. However, the union could make up the majority of GTV, e.g., up to 62% of GTV in our case, resulting in a possible increase in toxicity. The third possible approach is to adaptively boost the persisting union of the subvolumes after first two weeks of radiation treatment. Our and other data suggest that there would be approximately 40-50% of reduction in the subvolumes determined by the metabolic and physiological imaging risk factors, which could minimize toxicity.

In this study, we chose $SUV_{50\%max}$ as the threshold to define high FDG uptake subvolumes. Currently, there is no standard on how to define the target edge on FDG PET. Several segmentation methods were used widely, including thresholding with a fixed SUV (2.5), maximum tumor signal intensity (40% or 50%) and adaptive signal to background ratio.(49) We chose $SUV_{50\%max}$ as the threshold to bring in accordance with ongoing clinical trials.(7, 26, 50) To investigate the influence of different threshold methods, we also generated subvolumes by using $SUV_{30\%max}$, which did not alter our findings. Similarly, thresholds were used for determining the subvolumes of low BV and low ADC, for which we used the threshold values reported in literature and compared to our own data. Nevertheless, we performed voxel-level correlations that are independent of thresholds used, and led to the similar results.

There are some limitations in our study, particularly for separating effects of biology and target displacement errors on the poorer spatial correspondence of the image parameters. The ssEPI is sensitive to susceptibility effects, resulting in exclusion of seven patients who had median values of target displacement errors > 6 mm and severe artifacts from analysis. The RESOLVE sequence used to scan the last 16 patients permits the use of extremely short echo spacing to significantly improve image quality and geometric accuracy compared to the ssEPI.(23) As a result, there were no patients who had median target displacement errors greater than 4 mm. The analysis of whether the extent of image-parameter spatial correspondence was correlated with the extent of target displacement errors suggests that the

poorer spatial correspondence between image parameters cannot solely attribute to the target displacement error. Also, overlap volumes between image parameters are potentially influenced by segmentation methods. However, results from voxel-level analysis that is not affected by segmentation suggest the same poor spatial correspondence between image modalities.

Conclusion

FDG-PET, DCE-MRI and DWI as imaging risk factors in head-and neck cancer provide largely distinct spatial information and single imaging modality may be insufficient to define the target for dose boosting/painting in HNSCC. Analysis of the associations of failure patterns with pretreatment risk-factor images could info us how to define the target in the next clinical trials.

Acknowledgments

This work is supported in part by NIH/NCI 1U01CA183848 and RO1CA184153.

References

1. Overgaard J, Mohanti BK, Begum N, Ali R, Agarwal JP, Kuddu M, Bhasker S, Tatsuzaki H, Grau C. Five versus six fractions of radiotherapy per week for squamous-cell carcinoma of the head and neck (IAEA-ACC study): a randomised, multicentre trial. Lancet Oncol. 2010; 11:553–560. [PubMed: 20382075]
2. Chao KS, Ozyigit G, Tran BN, Cengiz M, Dempsey JF, Low DA. Patterns of failure in patients receiving definitive and postoperative IMRT for head-and-neck cancer. Int J Radiat Oncol Biol Phys. 2003; 55:312–321. [PubMed: 12527043]
3. Hermans R, Meijerink M, Van den Bogaert W, Rijnders A, Weltens C, Lambin P. Tumor perfusion rate determined noninvasively by dynamic computed tomography predicts outcome in head-and-neck cancer after radiotherapy. Int J Radiat Oncol Biol Phys. 2003; 57:1351–1356. [PubMed: 14630273]
4. Sovik A, Malinen E, Bruland OS, Bentzen SM, Olsen DR. Optimization of tumour control probability in hypoxic tumours by radiation dose redistribution: a modelling study. Phys Med Biol. 2007; 52:499–513. [PubMed: 17202629]
5. Vogelius IR, Hakansson K, Due AK, Aznar MC, Berthelsen AK, Kristensen CA, Rasmussen J, Specht L, Bentzen SM. Failure-probability driven dose painting. Med Phys. 2013; 40:081717. [PubMed: 23927314]
6. Wang J, Zheng J, Tang T, Zhu F, Yao Y, Xu J, Wang AZ, Zhang L. A Randomized Pilot Trial Comparing Position Emission Tomography (PET)-Guided Dose Escalation Radiotherapy to Conventional Radiotherapy in Chemoradiotherapy Treatment of Locally Advanced Nasopharyngeal Carcinoma. PLoS One. 2015; 10:e0124018. [PubMed: 25915944]
7. Madani I, Duthoy W, Derie C, De Gersem W, Boterberg T, Saerens M, Jacobs F, Gregoire V, Lonneux M, Vakaet L, et al. Positron emission tomography-guided, focal-dose escalation using intensity-modulated radiotherapy for head and neck cancer. Int J Radiat Oncol Biol Phys. 2007; 68:126–135. [PubMed: 17448871]
8. Overgaard J. Hypoxic modification of radiotherapy in squamous cell carcinoma of the head and neck–a systematic review and meta-analysis. Radiother Oncol. 2011; 100:22–32. [PubMed: 21511351]
9. Rasmussen JH, Hakansson K, Vogelius IR, Aznar MC, Fischer BM, Friborg J, Loft A, Kristensen CA, Bentzen SM, Specht L. Phase I trial of 18F-Fludeoxyglucose based radiation dose painting with concomitant cisplatin in head and neck cancer. Radiother Oncol. 2016; 120:76–80. [PubMed: 26993418]

10. Jansen JF, Schoder H, Lee NY, Stambuk HE, Wang Y, Fury MG, Patel SG, Pfister DG, Shah JP, Koutcher JA, et al. Tumor metabolism and perfusion in head and neck squamous cell carcinoma: pretreatment multimodality imaging with 1H magnetic resonance spectroscopy, dynamic contrast-enhanced MRI, and [18F]FDG-PET. Int J Radiat Oncol Biol Phys. 2012; 82:299–307. [PubMed: 21236594]
11. Soto DE, Kessler ML, Piert M, Eisbruch A. Correlation between pretreatment FDG-PET biological target volume and anatomical location of failure after radiation therapy for head and neck cancers. Radiother Oncol. 2008; 89:13–18. [PubMed: 18555547]
12. Yao M, Graham MM, Smith RB, Dornfeld KJ, Skwarchuk M, Hoffman HT, Funk GF, Graham SM, Menda Y, Buatti JM. Value of FDG PET in assessment of treatment response and surveillance in head-and-neck cancer patients after intensity modulated radiation treatment: a preliminary report. Int J Radiat Oncol Biol Phys. 2004; 60:1410–1418. [PubMed: 15590172]
13. Cao Y, Popovtzer A, Li D, Chepeha DB, Moyer JS, Prince ME, Worden F, Teknos T, Bradford C, Mukherji SK, et al. Early prediction of outcome in advanced head-and-neck cancer based on tumor blood volume alterations during therapy: a prospective study. Int J Radiat Oncol Biol Phys. 2008; 72:1287–1290. [PubMed: 19028268]
14. Due AK, Vogelius IR, Aznar MC, Bentzen SM, Berthelsen AK, Korreman SS, Loft A, Kristensen CA, Specht L. Recurrences after intensity modulated radiotherapy for head and neck squamous cell carcinoma more likely to originate from regions with high baseline [18F]-FDG uptake. Radiother Oncol. 2014; 111:360–365. [PubMed: 24993331]
15. Pollom EL, Song J, Durkee BY, Aggarwal S, Bui T, von Eyben R, Li R, Brizel DM, Loo BW, Le QT, et al. Prognostic value of midtreatment FDG-PET in oropharyngeal cancer. Head Neck. 2016; 38:1472–1478. [PubMed: 27043927]
16. Schwartz DL, Harris J, Yao M, Rosenthal DI, Opanowski A, Levering A, Ang KK, Trotti AM, Garden AS, Jones CU, et al. Metabolic tumor volume as a prognostic imaging-based biomarker for head-and-neck cancer: pilot results from Radiation Therapy Oncology Group protocol 0522. Int J Radiat Oncol Biol Phys. 2015; 91:721–729. [PubMed: 25752384]
17. Duprez F, De Neve W, De Gersem W, Coghe M, Madani I. Adaptive dose painting by numbers for head-and-neck cancer. Int J Radiat Oncol Biol Phys. 2011; 80:1045–1055. [PubMed: 20643512]
18. XXX (blinded).
19. Ng SH, Liao CT, Lin CY, Chan SC, Lin YC, Yen TC, Chang JT, Ko SF, Fan KH, Wang HM, et al. Dynamic contrast-enhanced MRI, diffusion-weighted MRI and 18F-FDG PET/CT for the prediction of survival in oropharyngeal or hypopharyngeal squamous cell carcinoma treated with chemoradiation. Eur Radiol. 2016; 26:4162–4172. [PubMed: 26911889]
20. Vaid S, Chandorkar A, Atre A, Shah D, Vaid N. Differentiating recurrent tumours from post-treatment changes in head and neck cancers: does diffusion-weighted MRI solve the eternal dilemma? Clin Radiol. 2017; 72:74–83. [PubMed: 27789026]
21. Kim S, Loevner L, Quon H, Sherman E, Weinstein G, Kilger A, Poptani H. Diffusion-weighted magnetic resonance imaging for predicting and detecting early response to chemoradiation therapy of squamous cell carcinomas of the head and neck. Clin Cancer Res. 2009; 15:986–994. [PubMed: 19188170]
22. www.clinicaltrials.gov. NCT01504815, NCT01283178, NCT01208883, NCT01341535, NCT00306294, NCT02352792, NCT00896350, NCT01212354, and NCT02089204.
23. Zhao M, Liu Z, Sha Y, Wang S, Ye X, Pan Y, Wang S. Readout-segmented echo-planar imaging in the evaluation of sinonasal lesions: A comprehensive comparison of image quality in single-shot echo-planar imaging. Magn Reson Imaging. 2016; 34:166–172. [PubMed: 26541548]
24. Daisne JF, Sibomana M, Bol A, Doumont T, Lonneux M, Gregoire V. Tridimensional automatic segmentation of PET volumes based on measured source-to-background ratios: influence of reconstruction algorithms. Radiother Oncol. 2003; 69:247–250. [PubMed: 14644483]
25. Tofts PS, Kermode AG. Measurement of the Blood-Brain-Barrier Permeability and Leakage Space Using Dynamic Mr Imaging .1. Fundamental-Concepts. Magnetic Resonance in Medicine. 1991; 17:357–367. [PubMed: 2062210]
26. Houweling AC, Wolf AL, Vogel WV, Hamming-Vrieze O, van Vliet-Vroegindeweij C, van de Kamer JB, van der Heide UA. FDG-PET and diffusion-weighted MRI in head-and-neck cancer

patients: implications for dose painting. Radiother Oncol. 2013; 106:250–254. [PubMed: 23395065]

27. Cacicedo J, Navarro A, Del Hoyo O, Gomez-Iturriaga A, Alongi F, Medina JA, Elicin O, Skanjeti A, Giammarile F, Bilbao P, et al. Role of fluorine-18 fluorodeoxyglucose PET/CT in head and neck oncology: the point of view of the radiation oncologist. Br J Radiol. 2016; 89:20160217. [PubMed: 27416996]
28. Ligtenberg H, Jager EA, Caldas-Magalhaes J, Schakel T, Pameijer FA, Kasperts N, Willems SM, Terhaard CH, Raaijmakers CP, Philippens ME. Modality-specific target definition for laryngeal and hypopharyngeal cancer on FDG-PET, CT and MRI. Radiother Oncol. 2017
29. Allai AS, Dulguerov P, Allaoua M, Haenggeli CA, El-Ghazi el A, Lehmann W, Slosman DO. Standardized uptake value of 2-[(18)F] fluoro-2-deoxy-D-glucose in predicting outcome in head and neck carcinomas treated by radiotherapy with or without chemotherapy. J Clin Oncol. 2002; 20:1398–1404. [PubMed: 11870185]
30. Rasmussen JH, Vogelius IR, Fischer BM, Friborg J, Aznar MC, Persson GF, Hakansson K, Kristensen CA, Bentzen SM, Specht L. Prognostic value of 18F-fludeoxyglucose uptake in 287 patients with head and neck squamous cell carcinoma. Head Neck. 2015; 37:1274–1281. [PubMed: 24801812]
31. Chang KP, Tsang NM, Liao CT, Hsu CL, Chung MJ, Lo CW, Chan SC, Ng SH, Wang HM, Yen TC. Prognostic significance of 18F-FDG PET parameters and plasma Epstein-Barr virus DNA load in patients with nasopharyngeal carcinoma. J Nucl Med. 2012; 53:21–28. [PubMed: 22213820]
32. Kao CH, Lin SC, Hsieh TC, Yen KY, Yang SN, Wang YC, Liang JA, Hua CH, Chen SW. Use of pretreatment metabolic tumour volumes to predict the outcome of pharyngeal cancer treated by definitive radiotherapy. Eur J Nucl Med Mol Imaging. 2012; 39:1297–1305. [PubMed: 22532254]
33. Romesser PB, Lim R, Spratt DE, Setton J, Riaz N, Lok B, Rao S, Sherman EJ, Schoder H, Lee NY. The relative prognostic utility of standardized uptake value, gross tumor volume, and metabolic tumor volume in oropharyngeal cancer patients treated with platinum based concurrent chemoradiation with a pre-treatment [(18)F] fluorodeoxyglucose positron emission tomography scan. Oral Oncol. 2014; 50:802–808. [PubMed: 25043882]
34. Chawla S, Kim S, Dougherty L, Wang S, Loevner LA, Quon H, Poptani H. Pretreatment diffusion-weighted and dynamic contrast-enhanced MRI for prediction of local treatment response in squamous cell carcinomas of the head and neck. AJR Am J Roentgenol. 2013; 200:35–43. [PubMed: 23255739]
35. Ng SH, Lin CY, Chan SC, Yen TC, Liao CT, Chang JT, Ko SF, Wang HM, Huang SF, Lin YC, et al. Dynamic contrast-enhanced MR imaging predicts local control in oropharyngeal or hypopharyngeal squamous cell carcinoma treated with chemoradiotherapy. PLoS One. 2013; 8:e72230. [PubMed: 23951300]
36. Shukla-Dave A, Lee NY, Jansen JF, Thaler HT, Stambuk HE, Fury MG, Patel SG, Moreira AL, Sherman E, Karimi S, et al. Dynamic contrast-enhanced magnetic resonance imaging as a predictor of outcome in head-and-neck squamous cell carcinoma patients with nodal metastases. Int J Radiat Oncol Biol Phys. 2012; 82:1837–1844. [PubMed: 21601373]
37. Hatakenaka M, Shioyama Y, Nakamura K, Yabuuchi H, Matsuo Y, Sunami S, Kamitani T, Yoshiura T, Nakashima T, Nishikawa K, et al. Apparent diffusion coefficient calculated with relatively high b-values correlates with local failure of head and neck squamous cell carcinoma treated with radiotherapy. AJNR Am J Neuroradiol. 2011; 32:1904–1910. [PubMed: 21778248]
38. Ohnishi K, Shioyama Y, Hatakenaka M, Nakamura K, Abe K, Yoshiura T, Ohga S, Nonoshita T, Yoshitake T, Nakashima T, et al. Prediction of local failures with a combination of pretreatment tumor volume and apparent diffusion coefficient in patients treated with definitive radiotherapy for hypopharyngeal or oropharyngeal squamous cell carcinoma. J Radiat Res. 2011; 52:522–530. [PubMed: 21905311]
39. Lambrecht M, Van Calster B, Vandecaveye V, De Keyzer F, Roebben I, Hermans R, Nuyts S. Integrating pretreatment diffusion weighted MRI into a multivariable prognostic model for head and neck squamous cell carcinoma. Radiother Oncol. 2014; 110:429–434. [PubMed: 24630535]
40. Ng SH, Lin CY, Chan SC, Lin YC, Yen TC, Liao CT, Chang JT, Ko SF, Wang HM, Chang CJ, et al. Clinical utility of multimodality imaging with dynamic contrast-enhanced MRI, diffusion-

weighted MRI, and 18F-FDG PET/CT for the prediction of neck control in oropharyngeal or hypopharyngeal squamous cell carcinoma treated with chemoradiation. PLoS One. 2014; 9:e115933. [PubMed: 25531391]

41. Noij DP, Pouwels PJ, Ljumanovic R, Knol DL, Doornaert P, de Bree R, Castelijns JA, de Graaf P. Predictive value of diffusion-weighted imaging without and with including contrast-enhanced magnetic resonance imaging in image analysis of head and neck squamous cell carcinoma. Eur J Radiol. 2015; 84:108–116. [PubMed: 25467228]
42. Barker JL Jr, Garden AS, Ang KK, O'Daniel JC, Wang H, Court LE, Morrison WH, Rosenthal DI, Chao KS, Tucker SL, et al. Quantification of volumetric and geometric changes occurring during fractionated radiotherapy for head-and-neck cancer using an integrated CT/linear accelerator system. Int J Radiat Oncol Biol Phys. 2004; 59:960–970. [PubMed: 15234029]
43. Marzi S, Pinnaro P, D'Alessio D, Strigari L, Bruzzaniti V, Giordano C, Giovinazzo G, Marucci L. Anatomical and dose changes of gross tumour volume and parotid glands for head and neck cancer patients during intensity-modulated radiotherapy: effect on the probability of xerostomia incidence. Clin Oncol (R Coll Radiol). 2012; 24:e54–62. [PubMed: 22138192]
44. Driessen JP, Caldas-Magalhaes J, Janssen LM, Pameijer FA, Kooij N, Terhaard CH, Grolman W, Philippens ME. Diffusion-weighted MR imaging in laryngeal and hypopharyngeal carcinoma: association between apparent diffusion coefficient and histologic findings. Radiology. 2014; 272:456–463. [PubMed: 24749712]
45. Driessen JP, van Bemmel AJ, van Kempen PM, Janssen LM, Terhaard CH, Pameijer FA, Willems SM, Stegeman I, Grolman W, Philippens ME. Correlation of human papillomavirus status with apparent diffusion coefficient of diffusion-weighted MRI in head and neck squamous cell carcinomas. Head Neck. 2016; 38(Suppl 1):E613–618. [PubMed: 25783872]
46. Nakahira M, Saito N, Yamaguchi H, Kuba K, Sugasawa M. Use of quantitative diffusion-weighted magnetic resonance imaging to predict human papilloma virus status in patients with oropharyngeal squamous cell carcinoma. Eur Arch Otorhinolaryngol. 2014; 271:1219–1225. [PubMed: 23880924]
47. Maeda M, Kato H, Sakuma H, Maier SE, Takeda K. Usefulness of the apparent diffusion coefficient in line scan diffusion-weighted imaging for distinguishing between squamous cell carcinomas and malignant lymphomas of the head and neck. AJNR Am J Neuroradiol. 2005; 26:1186–1192. [PubMed: 15891182]
48. Yun TJ, Kim JH, Kim KH, Sohn CH, Park SW. Head and neck squamous cell carcinoma: differentiation of histologic grade with standard- and high-b-value diffusion- weighted MRI. Head Neck. 2013; 35:626–631. [PubMed: 22605653]
49. Newbold K, Powell C. PET/CT in Radiotherapy Planning for Head and Neck Cancer. Front Oncol. 2012; 2:189. [PubMed: 23233906]
50. Madani I, Duprez F, Boterberg T, Van de Wiele C, Bonte K, Deron P, De Gersem W, Coghe M, De Neve W. Maximum tolerated dose in a phase I trial on adaptive dose painting by numbers for head and neck cancer. Radiother Oncol. 2011; 101:351–355. [PubMed: 21742392]

Summary

Several imaging risk biomarkers for treatment failure in head and neck cancer have been identified, largely in isolation. Understanding the spatial association between these imaging risk biomarkers is lacking, which could impact on decision making in clinical trials. This study found that high FDG uptake, low blood volume and low diffusion coefficient in head-and neck cancer identifies large distinct tumor subvolumes. Boosting target defined on a single imaging modality may not be adequate to achieve sufficient clinical benefits.

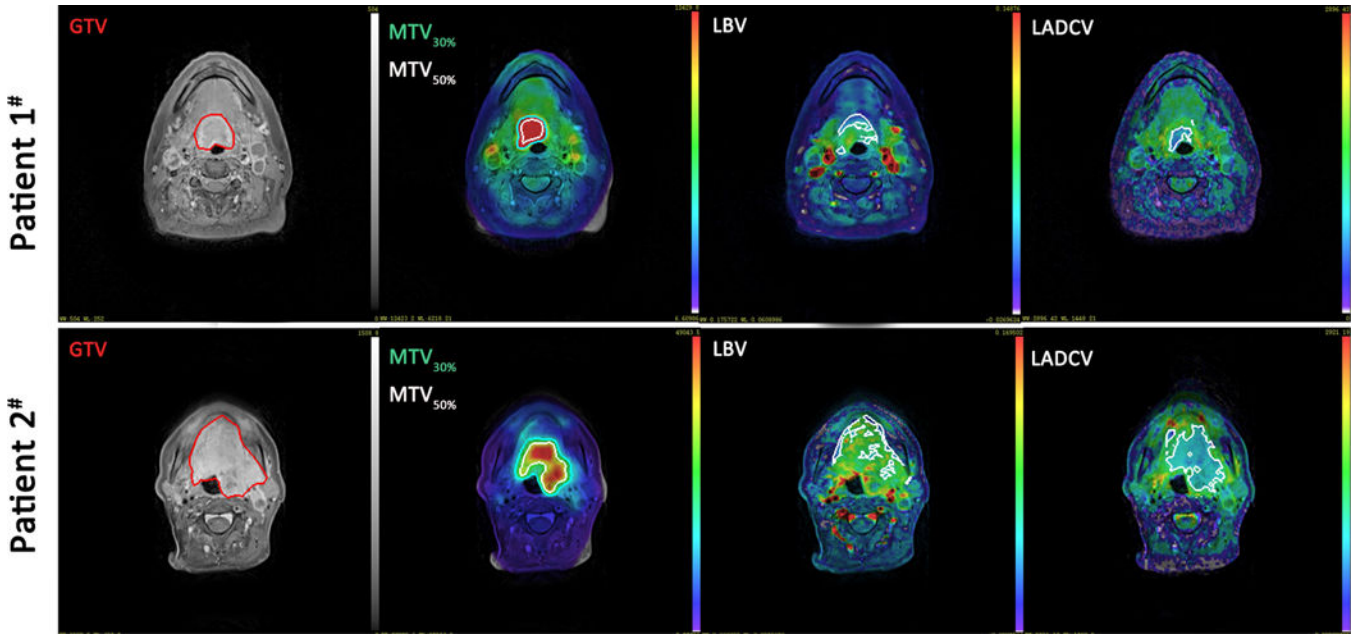

Figure 1.

Post-Gd T1-weighted (left), FDG-PET (second left), blood volume (second right), and ADC images (right) of two patients. MTV50% (white contour) and MTV30% (green contour) are metabolic tumor volumes thresholded above 50% and 30% of the maximum uptake, respectively (second left). LBV (white contour) is low blood volume of tumor (second right). LADCV (white contour) is low ADC volume of tumor (right). Red contours represent gross tumor volume.

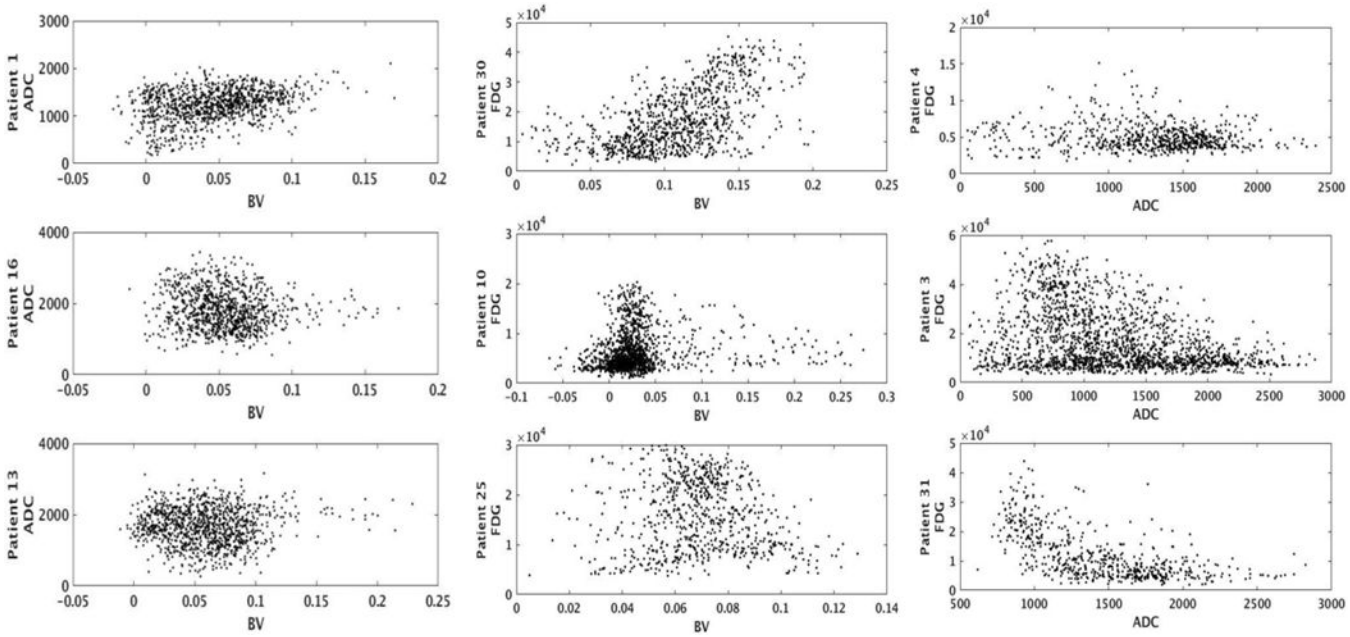

Figure 2.

Scatter plots of ADC vs BV (left column), FDG vs BV (middle column), and FDG vs ADC (right column row) in the GTVs for the patients who had the large positive (top), median (center), and largest negative (bottom) correlations.

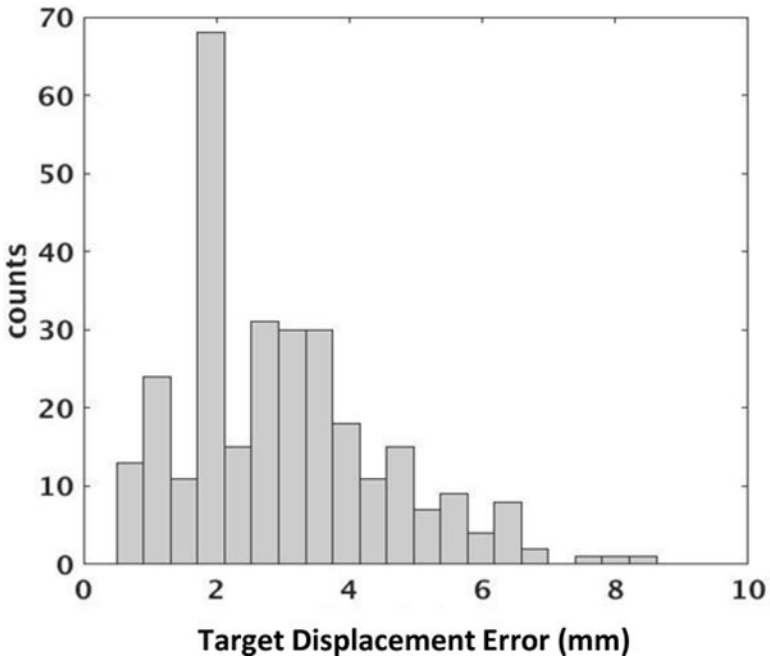

Figure 3.

Waterfall plots of Spearman's rank correlation coefficients between BV and ADC (left), between BV and FDG uptake (middle), and between ADC and FDG uptake (right).

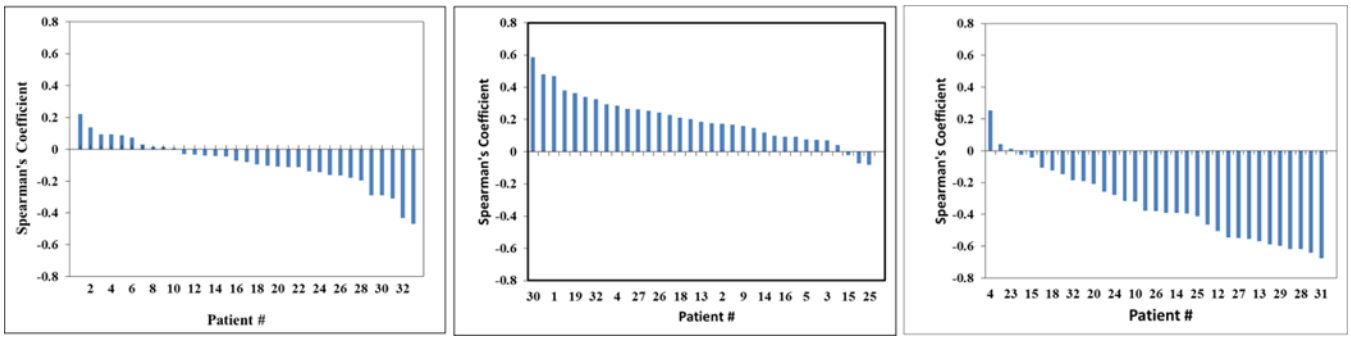

Figure 4.
A histogram of target displacement errors of all landmark points.

Table 1

Patient Characteristics

Characteristics	Number of Patients
Age: median (range) (years)	61(31-85)
Sex: male/female	35/5
Primary tumor site	
Oropharynx	27
Oral cavity	5
Nasopharynx	4
Hypopharynx	1
Larynx	1
Other	2
TN stage	
T4N3	4
T4N2	25
T4N1	1
T4N0	3
T3N3	1
T3N2	2
T2N3	1
T2N1	1
T1N3	1
Recurrent	1
Viral status (p16)	
Positive	23
Negative	14
Not known	3

Int J Radiat Oncol Biol Phys. Author manuscript; available in PMC 2019 November 15.

Table 2

GTV and image-phenotype subvolumes of primary tumor pre and after 2 weeks of CRT

	Pre-CRT		After 2 weeks of CRT		%Change 2Wks-pre
	Vol(cc)	%Subvol/GTV	Vol(cc)	%Subvol/GTV	
GTV	66.5 (10.2-595.2)	100	50.0 (6.9-368.9)	100	−19.6* (−45.5 - 16.1)
MTV	15.5 (2.2-259.7)	20.4 (4.1-98.9)	NA	NA	NA
LBV	12.1 (0.2-158.8)	21.3 (0.3-80.6)	6.2 (0.0-181.8)	13.2 (0.0-54.8)	−32.1* (−100 - 113.9)
LADC	24.3 (1.1-180.6)	45.1 (4.9-72.7)	7.7 (0.0-65.7)	16.1 (0.0-47.3)	−66.0** (−100—10.9)
Overlap(LBV, LADC)	2.0 (0.0-82.7)	3.4 (0.1-48.2)	0.5 (0.0-21.9)	1.1 (0.0-14.9)	−79.9* (−100 - 154.0)
Overlap(LBV, MTV)	1.5 (0-64.1)	2.2 (0.0-17.7)	NA	NA	NA
Overlap(LADC, MTV)	8.6 (0.6-59.0)	15.3 (1.6-41.2)	NA	NA	NA
Union(LBV,LADC)	34.6 (3.7-248.4)	56.7 (15.1-91.8)	15.2 (1.4-82.4)	28.2 (5.8-69.6)	−57.3* (−94.2 - −4.6)
Union(LBV, MTV)	24.3 (4.7-354.4)	43.5 (19.1-109.4)	NA	NA	NA
Union(LADC,MTV)	27.4 (4.1-188.8)	52.2 (14.3-100)	NA	NA	NA
Union(three)	41.3 (5.7-254.7)	64.4 (23.1-110.6)	NA	NA	NA

MTV: MTV_{50max}, metabolic tumor volume at 50% maximum; Union(three): union of LBV, LADC and MTV_{50max}. Median values (range) are given in each cell;

* p value < .05;

** p value <0.001.